




Melting Point of Pure Cr and Phase Equilibria in the Cr-Si Binary System

Kazushige Ioroi¹ · Yuki Aono¹ · Xiao Xu¹ · Toshihiro Omori¹  · Ryosuke Kainuma¹

Submitted: 25 February 2022 / Accepted: 27 March 2022 / Published online: 1 May 2022
© ASM International 2022

Abstract The melting point of pure Cr and phase equilibria in the Cr-Si binary system were determined by thermal analysis using a differential scanning calorimeter (DSC) and differential thermal analyzer (DTA). In addition, the composition of two-phase alloys was analyzed using an electron probe microanalyzer (EPMA). Heat treatment above 1500 °C was conducted in a high-frequency induction heating furnace, where the temperature was estimated by a two-color pyrometer with an accuracy of ± 20 °C. The melting point of pure Cr was determined to be 1861 ± 3 °C, considering the O and N impurities. The phase diagram of the Cr-Si system was determined in the whole composition range. The invariant reaction related to the formation of Cr₃Si and Cr₅Si₃ phases was confirmed as the eutectic reaction of liquid \leftrightarrow Cr₃Si + Cr₅Si₃. The solubility range of Cr₃Si phase is on the Cr-rich side from the stoichiometric composition, whereas the solubility range of Cr₅Si₃ phase extends toward the Si-rich side. We found using the x-ray diffraction that the α -Cr₅Si₃/ β -Cr₅Si₃ transformation does not exist.

Keywords chromium · chromium-silicon · experimental phase equilibria · high temperature materials · melting point · phase diagram

1 Introduction

Currently, novel high-temperature alloys based on refractory metals^[1,2] have attracted attention in the development of alloys beyond the Ni-based superalloys.^[3–6] Chromium (Cr) can be used as high-temperature material because it has a higher melting point and lower density than Ni. Cr-based alloys strengthened by the Laves phases, such as Cr-Nb^[7–10] and Cr-Ta^[11,12] alloys, exhibit excellent high-temperature strength. However, further improvement of their oxidation resistance and low-temperature brittleness is required. Si addition enhances both the nitridation and oxidation resistance of chromium, and the Cr-Si alloys show an excellent oxidation resistance.^[13,14] Recently, we found that the Cr-Si binary alloys have higher specific strength and oxidation resistance at high temperatures than those of Ni-based superalloy Mar-M247.^[15] In addition, the CrSi₂ phase has been investigated as thermoelectric material.^[16–18] An accurate phase diagram of the Cr-Si system can guide alloy design and heat treatment to enhance the properties of the Cr-Si alloys. However, for the phase diagrams including Cr, reliable experimental data are limited due to the difficulty of conducting the experiments at high temperatures. In this study, the melting point of pure Cr and phase equilibria in the Cr-Si binary system were experimentally investigated.

2 Literature Information

2.1 Melting Point of Pure Cr

The reported melting points are between 1842 and 1933 °C, which can be divided into three classes: ~ 1930 , ~ 1895 , and ~ 1850 °C. The melting points reported for

✉ Toshihiro Omori
omori@material.tohoku.ac.jp

¹ Department of Materials Science, Graduate School of Engineering, Tohoku University, 6-6-02 Aoba-yama, Sendai 980-8579, Japan

Table 1 Summary of experimental studies and recommended melting points for pure Cr

Melting point, °C	References	Year	First author	Method	Temperature measurement	Temperature calibration	Impurity	Comment
<i>Experiments</i>								
1890 ± 10	Ref. 24	1936	Grube	Thermal analysis	No description	Cu, Pd	No description	
1860 ± 20	Ref. 25	1949	Carille	Thermal analysis	Optical pyrometer	Ni	(1) 0.14% O, 0.011% N (2) 0.19% O, 0% N	Extrapolation to zero N, O content (1) 1845 °C (2) 1836 °C
1892	Ref. 26	1951	Putman	Thermal analysis	W-Mo thermocouple	No description	0.5% O	
1930	Ref. 27	1951	Bloom	Thermal analysis	W-Mo thermocouple	No description	0.06% O, 0.02% C	
1845 ± 10	Ref. 28	1951	Greenaway	Thermal analysis	W-Mo thermocouple	Optical pyrometer	0.045 mass% O, 0.038 mass% N	Extrapolation to zero N, O content
1903 ± 10	Ref. 30	1952	Bloom	Thermal analysis	W-Mo thermocouple	No description	0.008 % O, 0.002 % N	
1849 ± 20	Ref. 31	1959	Haworth	Heating method	Optical pyrometer	Mn, Ni, Pd, Pt, Rh, Ir	0.02–0.08 mass% O, 0.004 mass% N	
1893 ± 10	Ref. 32	1964	Pan	
1933	Ref. 33	1965	Nedumov	
1860 ± 6	Ref. 34	1967	Rudy	Pirani method	Optical pyrometer	Small black-body hole	0.0250 mass% O, 0.0250 mass% N	
1842 ± 20	Ref. 37	2001	Josell	Pulsed heat technique	Radiation thermometer		0.0076 mass% O	Computing from the measured emissivities and radiance temperatures using Planck's law
1861 ± 3	...	2021	This work	DTA	W-Re thermocouple	Ni, Pd, Pt	0.0508 mass% O, 0.0101 mass% N	
<i>Compilation</i>								
1857 ± 20	Ref. 22	1973	Hultgren					Compilation
1907 ± 20	Ref. 21	1982	Gurvich					Compilation accepted in SGTE
1863	Ref. 23	1992	Okamoto					ASM International

pure Cr are summarized in Table 1. The recommended melting point is different among compilations,^[21–23] and its true value is still under discussion.

The melting point, 1907 ± 20 °C, in the SGTE (Scientific Group Thermodata Europe)^[19] database is based on the assessment by Andersson,^[20] who adopted the value in a compilation published by Gurvich et al.^[21] Gurvich et al. chose the melting points of pure Cr reported by Grube and Knabe^[24] (1890 ± 10 °C), Putman et al.^[26] (1892 °C), Bloom et al.^[30] (1903 ± 10 °C), Pan^[32] (1893 ± 10 °C), and Nedumov and Grigorovich^[33] (1933 °C) as reliable data among the experimental information^[24–33] reported at that time, which lies in the highest and second-highest classes. Bloom et al.^[30] measured the melting point as 1903 ± 10 °C by thermal analysis using a tungsten-molybdenum

thermocouple and high purity samples having about 0.008% O, 0.002% N, and negligible carbon. In addition, Putman et al.^[26] investigated the melting point of Cr using a sample containing approximately 0.5% O using the same method.

However, Hultgren et al.^[22] suggested 1857 ± 20 °C based on the values by Carlile et al.^[25] (1860 ± 20 °C), Greenaway et al.^[28] (1845 ± 10 °C), and Haworth and Hume-Rothery^[31] (1849 ± 20 °C), which Gurvich et al. did not adopt. Carlile et al.^[25] measured the solidification temperature of pure Cr using an optical pyrometer calibrated using the melting point of pure Ni, and 1860 ± 20 °C was obtained after extrapolation to zero impurity content. Greenaway et al.^[28] conducted temperature measurement using a tungsten–molybdenum thermocouple and used an optical pyrometer for temperature calibration, from 1700 to 2200 °C. They also extrapolated to zero impurity content and estimated the melting point of pure Cr to be 1845 ± 10 °C. Haworth and Hume-Rothery^[31] determined the melting point of pure Cr to be 1849 ± 20 °C based on heating measurements using an optical pyrometer. They confirmed the measurement accuracy using the melting point of pure metals (Mn, Ni, Pd, Pt, Rh, and Ir), i.e., within ± 10 °C in the range of 1300–1800 °C, within ± 15 °C in the range of 1800–2300 °C, and within ± 20 °C in the range 2300 °C–2700 °C.

Recently, experimental investigations report the melting point of pure Cr to be 1860 ± 6 °C determined by Rudy and Windisch^[34] using the Pirani method^[35,36] and 1842 ± 20 °C determined by Josell et al.^[37] using the pulsed-heating technique. These values agree with the experimental data^[25,28,31] accepted in Hultgren et al.’s compilation.^[22] In addition, 1863 °C was recommended in the phase diagram compilation published by ASM International.^[23]

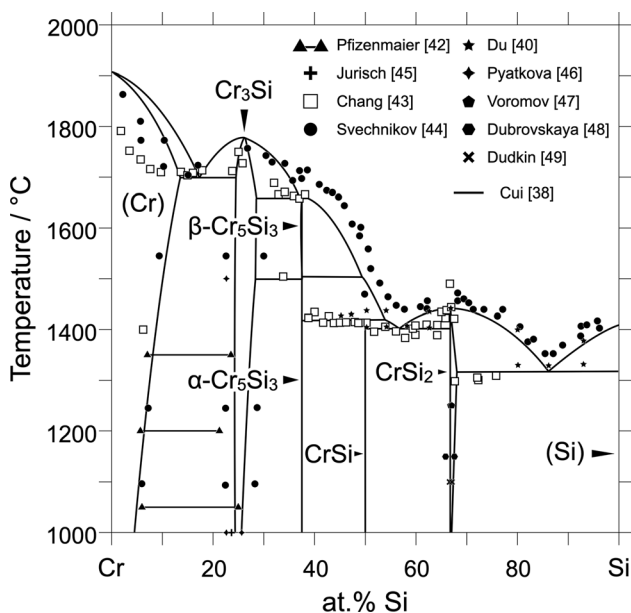


Fig. 1 Phase diagram of the Cr-Si binary system assessed by Cui and Jung^[38] using experimental data

Table 2 Summary of crystal structure information in the Cr-Si system

Phase	Space group	System	Prototype	Pearson symbol	Lattice parameters, nm			References
					a	b	c	
(Cr)	<i>Im-3m</i>	Cubic	W	cI2	0.2910	Ref. 50
Cr ₃ Si	<i>Pm-3n</i>	Cubic	Cr ₃ Si	cP8	0.45580	Ref. 45 51
β-Cr ₅ Si ₃
α-Cr ₅ Si ₃	<i>I4/mcm</i>	Tetragonal	W ₅ Si ₃	tI38	0.9170	0.4636	...	Ref. 52
CrSi	<i>P2₁3</i>	Cubic	FeSi	cP8	0.4620	Ref. 53
CrSi ₂	<i>P6₂22</i>	Hexagonal	CrSi ₂	hP9	0.442758	...	0.636805	Ref. 54
(Si)	<i>Fd-3m</i>	Diamond	C	cF8	0.54309	Ref. 55

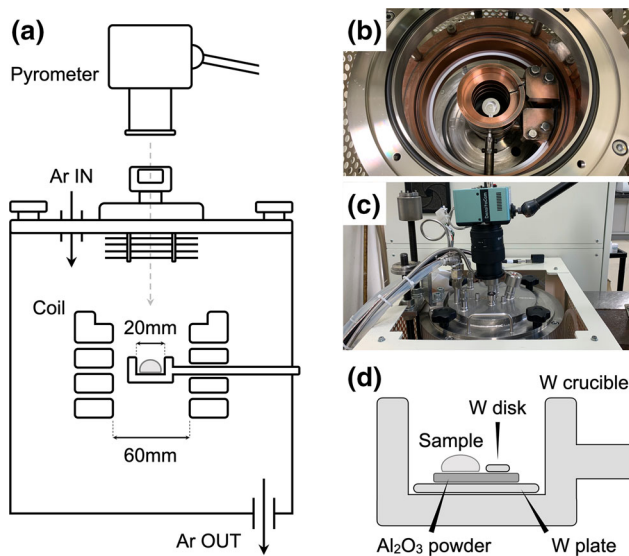


Fig. 2 (a) Schematic of a high-temperature furnace, (b) interior view of high-temperature furnace, (c) view during heat treatment using two-color pyrometer, and (d) schematic illustration around specimen designed in this work

2.2 Cr-Si Phase Diagram

Figure 1 shows the phase diagram of the Cr-Si binary system.^[38] The crystal structures of the constituent phases^[17,45,50–54] are in Table 2. The experimental data obtained by Chang^[43] and Svechnikov et al.^[44] have been used to evaluate the high Cr side. The solvus temperature of the Cr solid solution phase has been determined using metallography, X-ray diffraction (XRD), and differential thermal analysis (DTA). Transformation temperatures, including liquidus, solidus, and eutectic temperatures were determined using the Pirani method,^[35,36] which is a technique to determine the melting point of an alloy by optical observation. However, the results obtained using the Pirani method can be inaccurate at high temperatures because of the difficulty in observing the liquid as it forms. Besides, Du and Schuster^[40] have indicated that the transformation temperatures investigated by Chang^[43] may be affected by carbon contamination because of the graphite die used during the fabrication of the alloys. Thus, these experimental results may be lower than the actual melting point of Cr-Si.

Pyatkova et al.^[46] and Jurisch and Behr^[45] have measured the homogeneity range of the Cr₃Si phase at 1000 °C using the XRD and metallography. Regarding the Cr₅Si₃ phase, Chang^[43] has suggested that structural transformation occurred between the α -Cr₅Si₃ and β -Cr₅Si₃ phases based on the results of DTA measurements. Du and Schuster^[40] applied the thermodynamic model of Ti₅Si₃ to describe the β -Cr₅Si₃. However, the crystal structure and solubility range of the Cr₅Si₃ phase have not been reported.

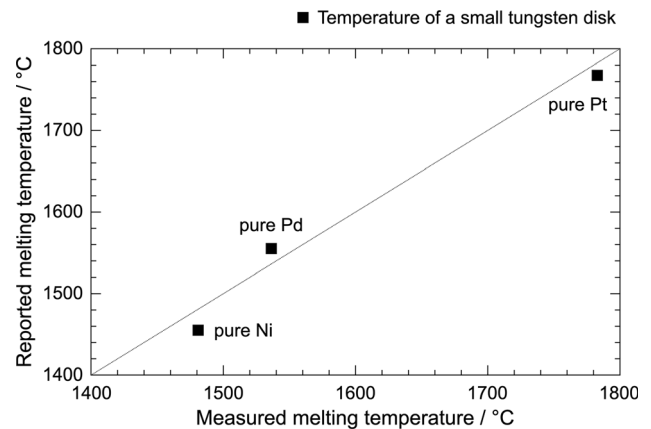


Fig. 3 Relation between measured and reported melting temperatures for estimation of temperature error in the present experiments

In addition, the invariant reaction consisting of liquid, Cr₃Si, and Cr₅Si₃ phases is under discussion. Recent thermodynamic evaluation by Chen et al.^[39] has suggested that this reaction is peritectic; however, some evaluations have accepted eutectic reaction.^[38,40,41]

The thermodynamic description of the phase diagram in the Cr-Si binary system has updated several times^[38–41]; the latest one assessed by Cui and Jung^[38] based on the experimental investigations^[43–49] is shown in Fig. 1. This phase diagram consists of four intermetallic compounds, Cr₃Si, Cr₅Si₃, CrSi, and CrSi₂, in addition to the Cr and Si solid solutions.

3 Experimental Procedure

3.1 Alloy Preparation

Cr-Si alloys were made from high purity Cr (99.99%) and Si (99.999%). The impurity contents of Cr were measured using an inductively coupled plasma optical emission spectrometer (ICP-OES) to be 0.0147 mass% O, 0.0003 mass% N, 0.0022 mass% C, 0.0002 mass% S, less than 0.01 mass% P and Si, and less than 0.003 mass% Al, Cu, and Fe. Button ingots were prepared by arc melting in Ar gas atmosphere using a nonconsumable tungsten electrode on a copper hearth. The ingots were melted seven times to ensure chemical homogeneity. As-cast ingots were cut into pieces, and the surface was ground to remove the oxidized layer. The alloy composition is denoted as at% unless noted.

In this study, a pure W (99.9%) plate with a thickness of 0.5 mm was used as the reference sample for measuring specimen temperature using the pyrometer. Some disk samples were cut out of the W plate, and the surface of the disk was ground.

3.2 Heat Treatment

Each specimen for examining phase equilibria at temperatures between 1200 and 1400 °C was encapsulated in a

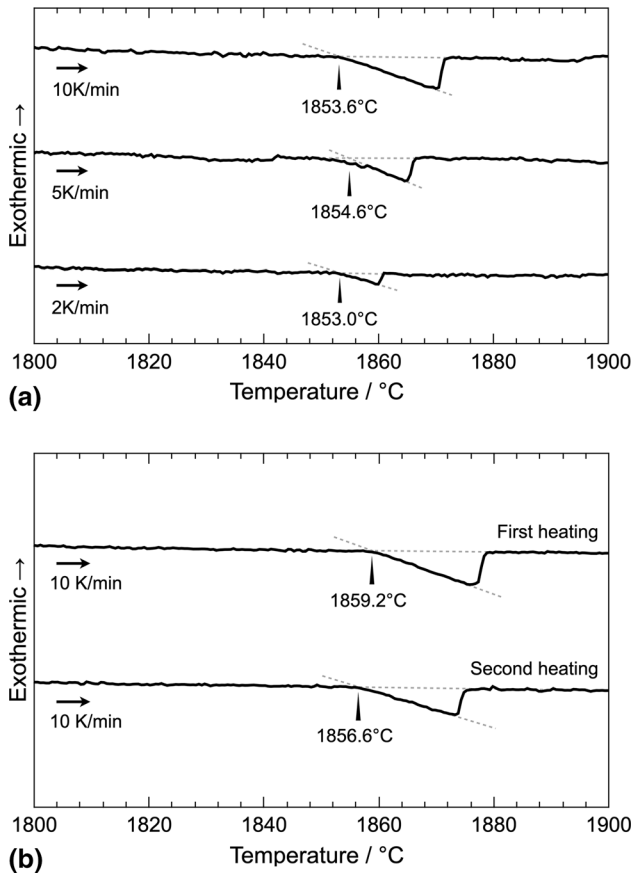


Fig. 4 (a) DTA heating curves measured for pure Cr with a heating rate of 2, 5, and 10 °C/min, and (b) heating rate of 10 °C/min for two-cycle under He atmosphere

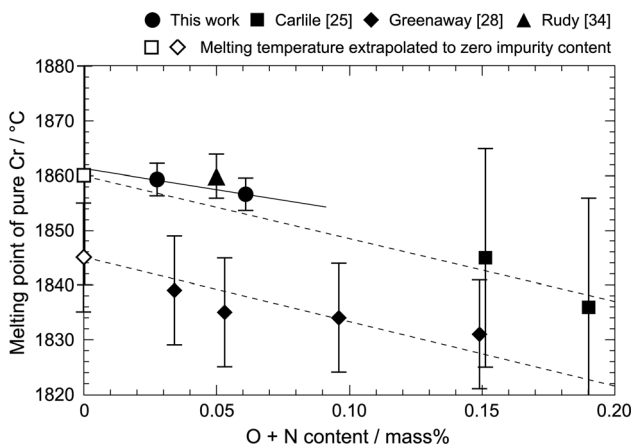


Fig. 5 Correlation between the melting point of pure Cr and impurity (O and N) contents measured using ICP-OES

quartz glass tube refilled with Ar gas. Then, it was heat-treated in electric resistance heating furnaces, followed by quenching in iced water. The Cr-Si alloys may react with the quartz glass tube (SiO₂) because of the high oxygen affinity of Si. Therefore, during the heat treatment, Cr-Si alloys were separated from the quartz glass tube using tungsten wire twined around the sample.

The heat treatment for equilibration at 1500 and 1600 °C was conducted in a high-frequency induction heating furnace under a high purity Ar gas atmosphere. Figures 2(a) and (b) show the schematic and interior view of the furnace, respectively. The temperature was measured using a two-color pyrometer through the sapphire glass window, as shown in Fig. 2(c). In addition, we separated the Cr-Si specimen (3.5 × 5.5 × 1.5 mm) and tungsten reference sample (3.2 φ × 0.5 mm) using a thin Al₂O₃ powder layer (about 1-mm thickness), laid on the top of a tungsten plate (17.0 φ × 0.5 mm), and this setup was placed in a tungsten crucible, as illustrated in Fig. 2(d). The tungsten plate and Al₂O₃ powder were used to avoid crucible contaminations and heat treatment reactions, respectively. It was difficult to obtain an accurate temperature of the Cr-Si alloys because of surface changes during the heat treatment due to evaporation of Cr. Therefore, we measured the temperature of the nearby tungsten reference sample instead. The error in this method was estimated by measuring the melting points of Ni (99.9%, *T_m* = 1455.0 °C), Pd (99.9%, *T_m* = 1554.8 °C), and Pt (99.9%, *T_m* = 1768.3 °C). Each pure metal was heated using a tungsten reference sample at about 10 °C/min in the furnace, and the temperatures of both pure metal and tungsten reference

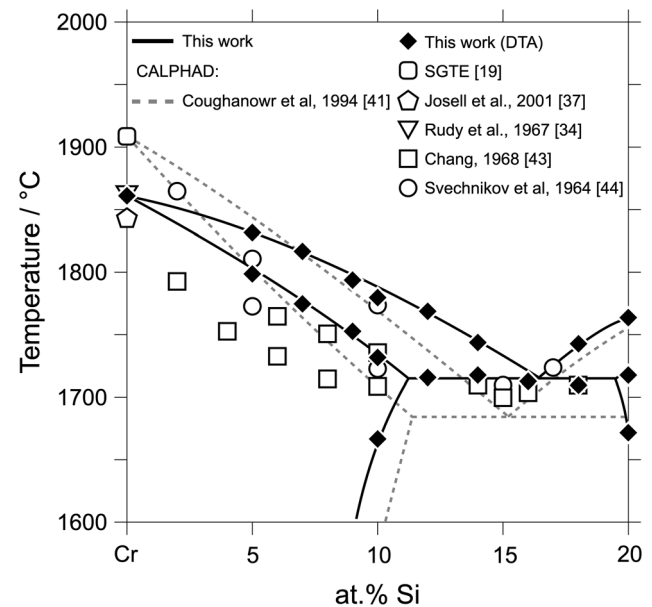


Fig. 6 Cr-rich portion of phase equilibria in high-temperature range of the Cr-Si system

samples were monitored. The temperatures of the tungsten reference samples were recorded when the melting temperatures of the pure metals were detected from the temperature-time curves; they are plotted against the accepted melting temperatures of pure metals in Fig. 3. The results indicate that the temperature accuracy is within ± 20 °C, which can be used as a thermometer in heat treatments conducted at high temperatures. The specimens heat-treated at 1500 and 1600 °C were furnace-cooled after switching off the high-frequency induction current, where the cooling rate was about 25 °C/s at high temperatures, between 1600 and 1200 °C.

3.3 Measurements of Equilibrium Compositions

The chemical compositions of the equilibrium phases were measured using a field-emission electron probe microanalyzer (FE-EPMA: JEOL JXA-8500F) equipped with a wavelength-dispersive-x-ray spectroscopy (WDS), with a 20-kV accelerating voltage and 10-nA beam current. The concentrations were measured from ten points per phase

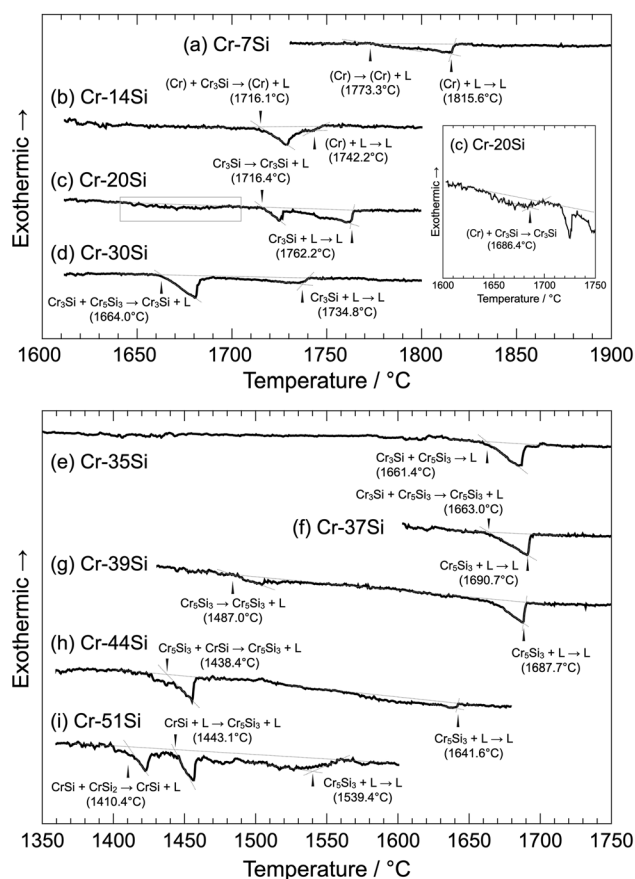


Fig. 7 DTA heating curves measured for (a) Cr-7Si, (b) Cr-14Si, (c) Cr-20Si, (d) Cr-30Si, (e) Cr-35Si, (f) Cr-37Si, (g) Cr-39Si, (h) Cr-44Si, and (i) Cr-51Si alloys at a heating rate of 10 °C/min under He gas atmosphere

and averaged without the maximum and minimum values. In addition, line analysis across an interphase boundary was conducted to confirm the absence of a composition gradient to ensure the equilibrium state.

3.4 Determination of Transformation Temperatures

Phase transformation temperatures in the Si-rich portion were determined using a differential scanning calorimeter (DSC: Netzsch DSC-404C). The DSC measurement was performed using an Al₂O₃ pan capped with an Al₂O₃ lid at a heating and cooling rate of 10 °C/min in Ar gas flow, and the temperature calibration using high purity Sn (99.99%, $T_m = 231.9$ °C), Al (99.99%, $T_m = 660.1$ °C), Ag (99.99%, $T_m = 951.5$ °C), Au (99.9%, $T_m = 1063.0$ °C), and Ni (99.99%, $T_m = 1455.0$ °C) was applied. The oxygen trap system (Netzsch OTS[®]) was employed to reduce the harmful effect of residual oxygen.

However, phase transformation temperatures in the Cr-rich portion, where the temperature is high, were investigated using a differential thermal analyzer (DTA: Netzsch STA 449 F3 Jupiter). The DTA measurement was performed in a static atmosphere of high purity He to prevent the evaporation of Cr. Each sample was placed on Al₂O₃ powder in a tungsten crucible with a tungsten lid. The effect of heating and cooling rates were examined at 2, 5, and 10 °C/min for pure Cr, whereas all other samples were measured at a heating and cooling rate of 10 °C/min. The calibration at different rates were conducted using high purity Ni (99.9%, $T_m = 1455.0$ °C), Pd (99.9%, $T_m = 1554.8$ °C), and Pt (99.9%, $T_m = 1768.3$ °C).

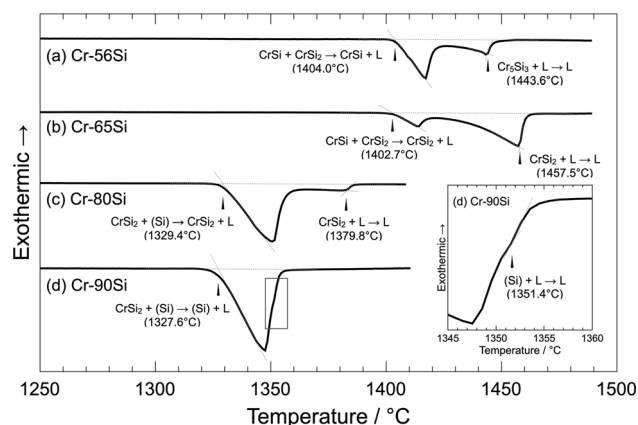
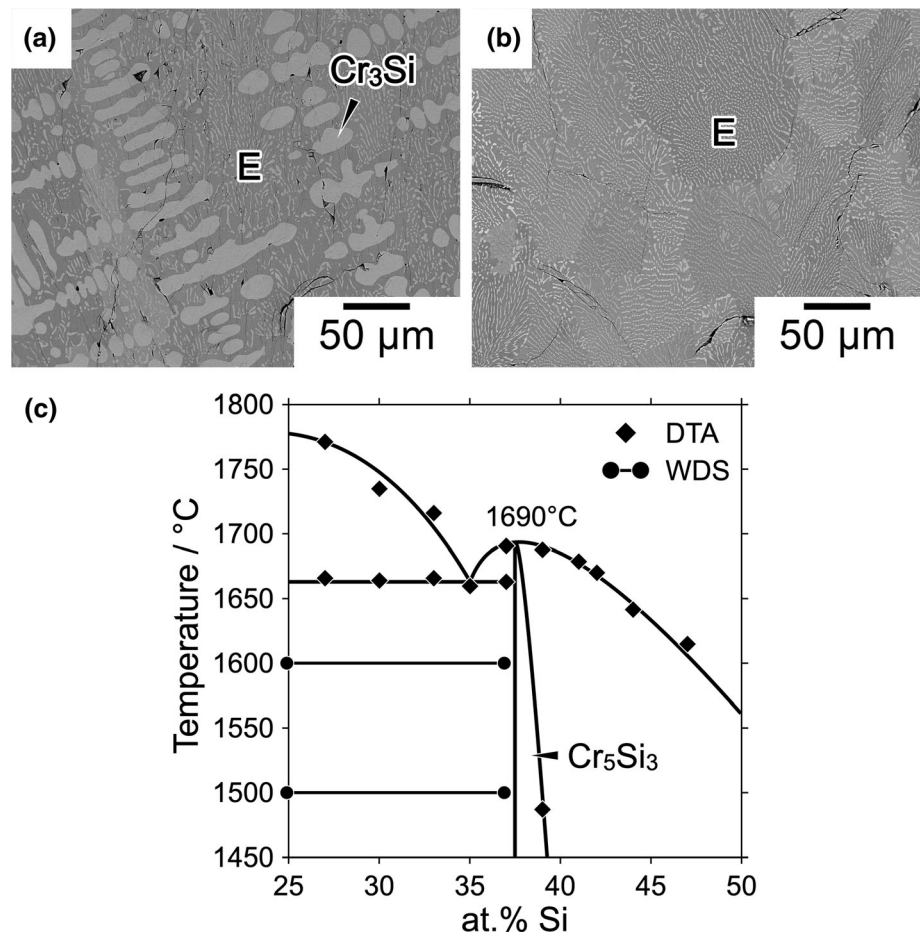


Fig. 8 DSC heating curves for (a) Cr-56Si, (b) Cr-65Si, (c) Cr-80Si, and (d) Cr-90Si alloys at a heating rate of 10 °C/min under an Ar gas atmosphere

Fig. 9 Back-scattered electron (BSE) images of as-cast microstructure of (a) Cr-33Si (b) Cr-35Si (at.%) alloys. “E” represents eutectic microstructure. (c) Phase diagram related to melting of Cr_5Si_3 phase in the Cr-Si system



4 Result and Discussion

4.1 Melting Point of Pure Cr

Figure 4(a) shows the DTA profiles of pure Cr obtained through measurements at heating rates of 2, 5, and 10 °C/min. The melting points, defined as the onset of the peaks, were close for all heating rates, suggesting that the dependence on the heating rate is negligible. In addition, the DTA heating and cooling measurement at a rate of 10 °C/min were repeated twice; the heating curves are shown in Fig. 4(b). The melting point in the first and second heating cycles were 1859.2 and 1856.6 °C, respectively. This decrease in melting point is due to increased impurity during the measurement. The ICP-OES revealed that the sum of O and N contents in Cr, before and after the DTA measurement, including melting is 0.0274 mass% (0.0196 mass% O and 0.0078 mass% N), and 0.0610 mass% (0.0509 mass% O and 0.0101 mass% N), respectively. The melting points obtained by Carlile et al.^[25] and Greenaway et al.,^[28] as well as this study, are plotted against the impurity (O + N) contents in Fig. 5. The slope of the three sets of data is similar. The results in this study

are close to the line by Carlile et al.,^[25] and the melting point of pure Cr is extrapolated to be 1861 °C. Moreover, the DTA measurements were conducted six times, and the uncertainties associated with the measurements were within ± 3 °C. Therefore, we concluded that the melting point of Cr is 1861 ± 3 °C, which is close to the values reported by Rudy and Windisch (1860 ± 4 °C).³⁴

Previous reports and this work focused on liquidus and solidus in the Cr-rich portion of the Cr-Si system are plotted in Fig. 6. As shown in this figure, the melting point of pure Cr accepted in SGTE (1907 °C)^[19] is consistent with the liquidus and solidus temperature of the Cr solid solution phase by Svechnikov et al.^[44] However, it is about 50 °C higher than the values measured by Rudy and Windisch,^[34] Josell et al.,^[37] and this study, and it is inconsistent with the liquidus and solidus investigated by Chang^[43] and Svechnikov et al.,^[44] as well as this study. A similar tendency has been observed in the Cr-Fe binary system. Xiong et al.^[55] have pointed out that in the Cr-Fe system, there is a large discrepancy between the experimental solidus and liquidus lines and the melting temperature of pure Cr in the SGTE and that the temperature of SGTE may be too high. The melting point accepted in

Table 3 Transformation temperatures determined by DTA and DSC analysis

Nominal composition of sample, at.% Si	Temperature, °C	Transformation during heating	Method
5	1797.0	(Cr) → (Cr) + L	DTA
	1830.7	(Cr) + L → L	
7	1773.3	(Cr) → (Cr) + L	
	1815.6	(Cr) + L → L	
9	1750.6	(Cr) → (Cr) + L	
	1791.9	(Cr) + L → L	
10	1665.8	(Cr) + Cr ₃ Si → (Cr)	
	1730.4	(Cr) → (Cr) + L	
	1778.1	(Cr) + L → L	
12	1714.3	Cr ₃ Si → (Cr) + L	
	1766.7	(Cr) + L → L	
14	1716.1	Cr ₃ Si → (Cr) + L	
	1742.2	(Cr) + L → L	
16	1711.4	Cr ₃ Si → (Cr) + L	
18	1708.1	(Cr) → Cr ₃ Si + L	
	1741.2	Cr ₃ Si + L → L	
20	1686.4	(Cr) + Cr ₃ Si → Cr ₃ Si	
	1716.4	Cr ₃ Si → Cr ₃ Si + L	
	1762.2	Cr ₃ Si + L → L	
22	1483.9	(Cr) + Cr ₃ Si → Cr ₃ Si	
	1755.0	Cr ₃ Si → Cr ₃ Si + L	
27	1665.4	Cr ₅ Si ₃ → Cr ₃ Si + L	
	1771.1	Cr ₃ Si + L → L	
30	1664.0	Cr ₅ Si ₃ → Cr ₃ Si + L	
	1734.8	Cr ₃ Si + L → L	
33	1665.8	Cr ₅ Si ₃ → Cr ₃ Si + L	
	1715.7	Cr ₃ Si + L → L	
35	1661.4	Cr ₅ Si ₃ + Cr ₃ Si → L	
37	1663.0	Cr ₃ Si → Cr ₅ Si ₃ + L	
	1690.7	Cr ₅ Si ₃ + L → L	
39	1487.0	Cr ₅ Si ₃ → Cr ₅ Si ₃ + L	
	1687.7	Cr ₅ Si ₃ + L → L	
41	1442.8	CrSi → Cr ₅ Si ₃ + L	
	1678.7	Cr ₅ Si ₃ + L → L	
42	1443.8	CrSi → Cr ₅ Si ₃ + L	
	1670.0	Cr ₅ Si ₃ + L → L	
44	1438.4	CrSi → Cr ₅ Si ₃ + L	
	1641.6	Cr ₅ Si ₃ + L → L	
47	1444.1	CrSi → Cr ₅ Si ₃ + L	
	1614.9	Cr ₅ Si ₃ + L → L	
51	1410.4	CrSi ₂ → CrSi + L	
	1443.1	CrSi → Cr ₅ Si ₃ + L	
	1539.4	Cr ₅ Si ₃ + L → L	
56	1404.0	CrSi ₂ → CrSi + L	DSC
	1443.6	CrSi + L → L	
60	1404.5	CrSi → CrSi ₂ + L	
	1435.1	CrSi ₂ + L → L	
65	1402.7	CrSi → CrSi ₂ + L	

Table 3 continued

Nominal composition of sample, at.% Si	Temperature, °C	Transformation during heating	Method
80	1457.5	CrSi ₂ + L → L	
	1460.5	CrSi ₂ + L → L	
	1329.4	(Si) → CrSi ₂ + L	
	1379.8	CrSi ₂ + L → L	
90	1327.6	CrSi ₂ → (Si) + L	
	1351.4	(Si) + L → L	
95	1327.0	CrSi ₂ → (Si) + L	
	1404.0	(Si) + L → L	

Table 4 Summary of invariant reaction temperatures determined by DTA and DSC measurements

Reaction type	Invariant reaction	Temperature, °C	References
Eutectic	(Cr) + Cr ₃ Si = Liquid	1715	This work
		1705 ± 5	43
Eutectic	Cr ₃ Si + Cr ₅ Si ₃ = Liquid	1665	This work
		1660 ± 10	43
Peritectic	Cr ₅ Si ₃ + CrSi = Liquid	1442	This work
		1413 ± 5	43
		1425 ± 4	40
Eutectic	CrSi + CrSi ₂ = Liquid	1404	This work
		1390 ± 10	43
		1404 ± 4	40
Eutectic	CrSi ₂ + (Si) = Liquid	1329	This work
		1305 ± 10	43
		1328 ± 1	40

SGTE is based on the reported values.^[24,26,30,32,33] However, it seems that aging of the thermocouples affected the temperature measurement,^[27,29] and temperature calibration might be insufficient although much information is not written. Recently, the melting point of 1863°C has been recommended for pure Cr,^[55,56] relying on the experimental data by Rudy and Windisch^[34] and Josell et al.^[37] and the phase diagram by ASM International.^[23] The result of this study supports these recent recommendations but determined the melting point to be 1861 ± 3 °C through careful experiments.

4.2 Thermal Analysis

The decrease in the melting point of pure Cr due to the contamination by O and N during the measurements was 2°C as shown in Fig. 5. This is considered to be the largest possible error in the Cr-Si system in the present work, because the highest reaction temperatures in Cr-Si alloys were lower than the melting point of pure Cr and Si is

expected to make the samples more protective to oxygen and nitrogen. Therefore, the effect of O + N content on the phase diagram is negligible small in the Cr-Si binary system and the measured results are directly used in the binary system.

Experimental results of phase transformation temperatures determined using the heating curves of DTA and DSC (Figs. 7 and 8) and the chemical composition analyses using the FE-EPMA/WDS (Figs. 9-11) are summarized in Fig. 12. The phase diagram assessed by Cui and Jung^[38] is superimposed with gray curves. Fig. 7 shows the DTA heating curves at a heating rate of 10 °C/min. In the Cr-7Si alloy shown in Fig. 7(a), a gradual fall and a tail can be recognized in the endothermic signal, corresponding to the solidus and liquidus temperatures, respectively. A sharp endothermic peak at around 1716 °C, followed by a small tail in Cr-14Si alloy shown in Fig. 7(b), is caused by the eutectic reaction of (Cr) + Cr₃Si ↔ L. The solvus temperature of the Cr solid solution phase is determined by the tail of the endothermic peak at 1686 °C, as shown in the

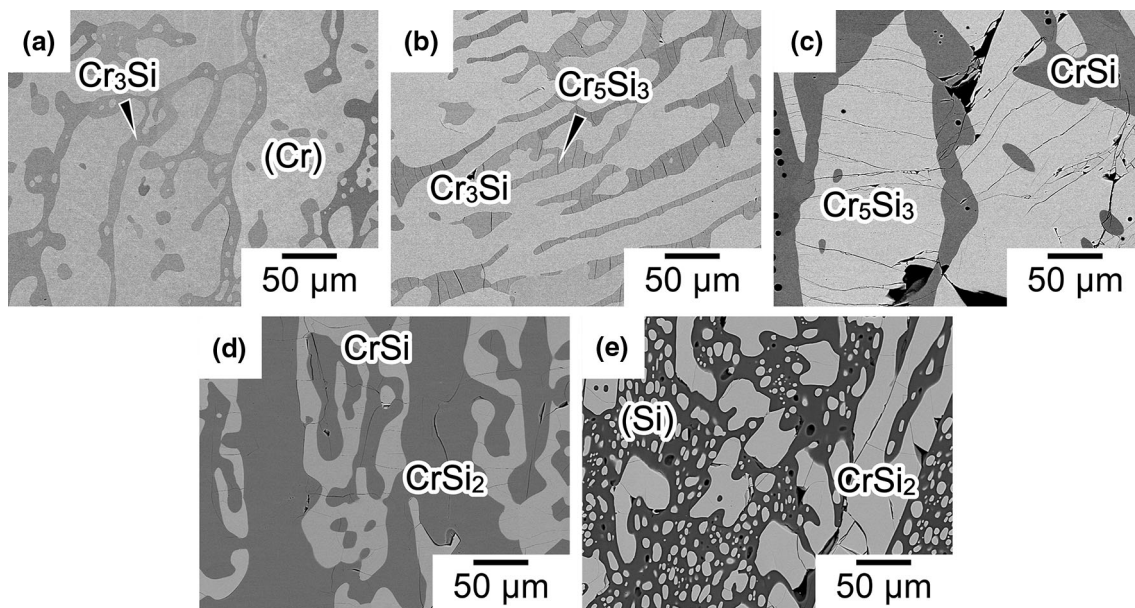
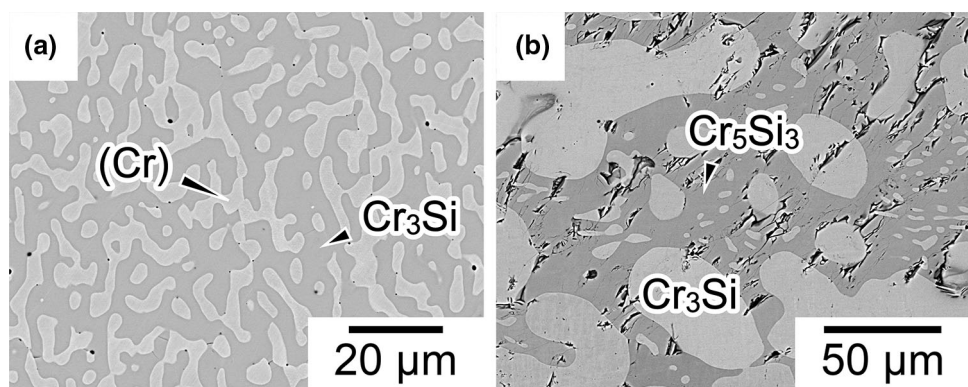


Fig. 10 Back-scattered electron (BSE) images of (a) Cr-12Si, (b) Cr-31Si and (c) Cr-44Si heat-treated at 1400 °C for 293 h and (d) Cr-61Si and (e) Cr-80Si heat-treated at 1300 °C for 336 h

Fig. 11 Back-scattered electron (BSE) images of (a) Cr-16Si heat-treated at 1600 °C for 3 h and (b) Cr-30Si heat-treated at 1500 °C for 15 h.



curve in Fig. 7(c). For the other alloys, the transformation temperatures are determined using the same method.

Figure 8 shows the DSC measurement results for alloys with high Si contents. The sharp endothermic signals are recognized in the curves, corresponding to the eutectic reaction and liquidus temperatures.

The transformation temperatures determined by DTA, and DSC measurements are in Table 3 and plotted in Fig. 12. The invariant temperatures coincide with the values obtained in the previous works (Table 4), except for the peritectic temperature consisting of liquid, Cr_5Si_3 , and CrSi phase. The revised peritectic temperature (1442 °C) is about 20 °C higher than the previous values (1413 ± 5 °C^[43] and 1425 ± 4 °C^[40]), as shown in Table 4. The liquidus temperatures are also higher than the previous

ones, as shown in Fig. 12. The congruent melting temperature of the CrSi_2 phase is higher than the experimental value by Du and Schuster (1439 °C)^[40]; however, it is in good agreement with that by Chang (1490 ± 20 °C)^[43]

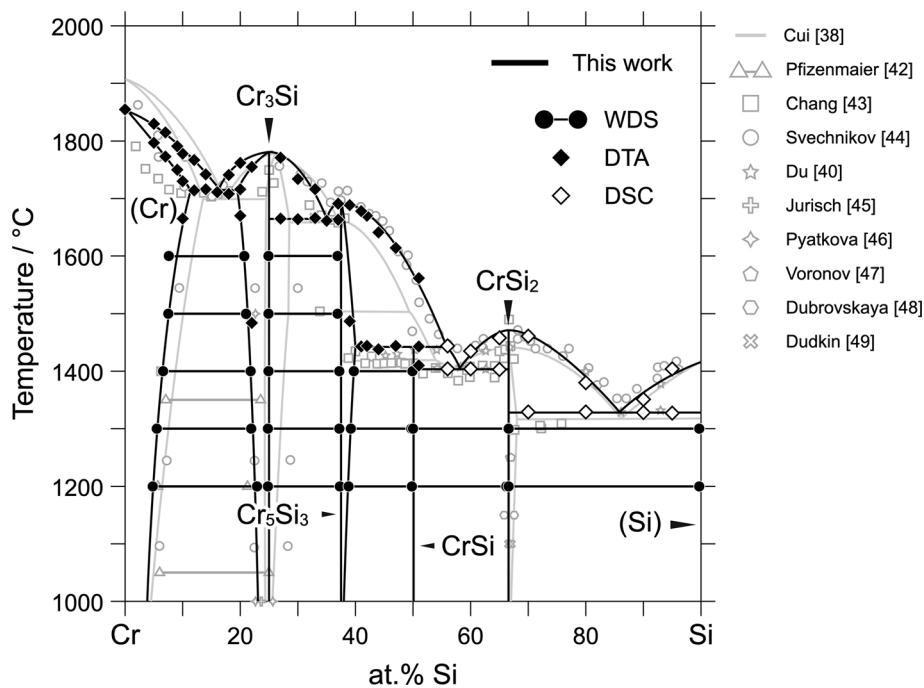
4.3 Reaction around Cr_5Si_3 Phase

There has been a discussion whether the invariant reaction related to the Cr_5Si_3 phase (the stoichiometric composition is Cr-37.5Si) is eutectic^[38,40,41] or peritectic.^[39,51] Figures 9(a) and (b) show as-cast microstructures of Cr-33Si and Cr-35Si alloys. Fine lamellar microstructure, with primary Cr_3Si phase and fully lamellar microstructure, are observed in Cr-33Si and Cr-35Si alloys, respectively. Based on these microstructures, we concluded that the

Table 5 Equilibrium compositions of Cr-Si alloys measured by FE-EPMA

Equilibrium phases		Nominal composition, at.% Si	Final heat-treatment condition for equilibration		Equilibrium composition, at.% Si	
phase1	phase2		Temp., °C	Time, h	Phase1	Phase2
(Cr)	Cr ₃ Si	16.0	1600	3	7.6	20.7
			1500	8	7.5	21.0
		12.0	1400	293	6.6	21.8
			1300	504	5.6	22.3
			1200	720	4.8	22.9
Cr ₃ Si	Cr ₅ Si ₃	30.0	1600	3	24.9	36.9
			1500	15	24.9	36.9
		31.0	1400	293	24.9	37.2
			1300	336	24.8	37.2
			1200	720	24.6	36.9
Cr ₅ Si ₃	CrSi	44.0	1400	293	39.7	49.9
			1300	336	39.2	49.7
		1200	720	38.4	50.1	
CrSi	CrSi ₂	61.0	1300	336	50.0	66.5
			1200	336	49.8	66.2
CrSi ₂	(Si)	80.0	1300	336	66.6	99.7
			1200	336	66.5	99.7

Fig. 12 Experimentally determined phase diagram of the Cr-Si system



invariant reaction, involving the Cr₃Si, Cr₅Si₃, and liquid phases, is eutectic, and eutectic composition is close to Cr-35Si. Moreover, the liquidus temperatures by DTA support this conclusion, as shown in Fig. 9(c). The liquidus

temperatures for Cr-37Si alloy (1690.7 °C) and Cr-39Si alloy (1687.7 °C) are almost equal, indicating that the congruent temperature of Cr₅Si₃ is about 1690 °C as depicted in Fig. 9(c).

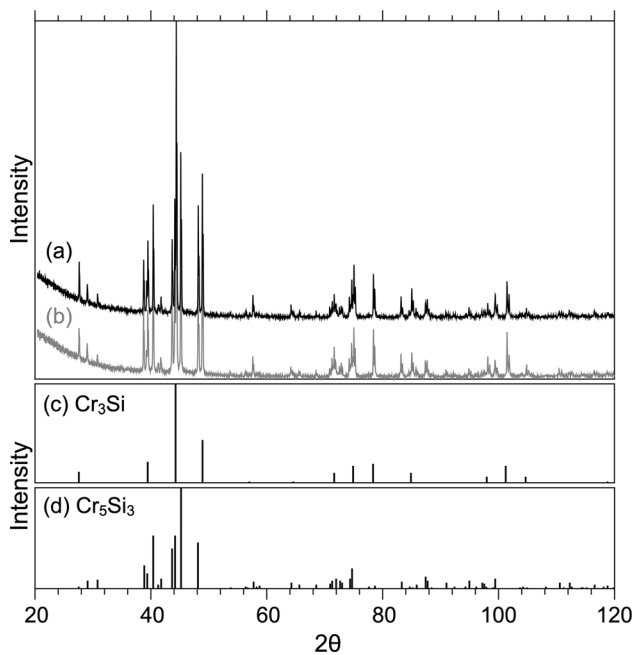


Fig. 13 Powder XRD patterns of Cr-33Si heat-treated at (a) 1600 °C 4 h and (b) 1300 °C 7 days using Cu K α radiation at room temperature. Calculated XRD patterns of (c) Cr₃Si and (d) Cr₅Si₃

4.4 Equilibrium Composition of Two-Phase Alloys

Figures 10 and 11 show the two-phase microstructures for alloys heat-treated at 1300 to 1600 °C. The specimens show a two-phase structure that is coarsened to over 10 μm , which is sufficient for quantitative analysis using FE-EPMA/WDS. The equilibrium data are in Table 5 and plotted in Fig. 12 with previous key experimental data^[40,42–49] and assessed phase diagram by Cui and Jung.^[38] In this study, the phase boundaries determined using thermal analysis and FE-EPMA/WDS measurements correlate with the phase boundaries of Cr solid solution and Cr₃Si phases.

Compared to the reported phase equilibria, we found that the Cr solid-solution phase has lower solubility of Si than those reported in past studies^[38,42,44] (Fig. 12). According to the phase diagram assessed by Cui and Jung,^[38] the solubility range of the Cr₃Si phase inclines toward the Si-rich side as temperature increases. The α -Cr₅Si₃ phase is treated as a line compound and the β -Cr₅Si₃ phase has a narrow solubility range because of insufficient experimental data. However, in that study, it was revealed that the Cr₃Si single-phase region inclines toward the Cr-rich side as temperature increases, which agrees with the reports by Svechnikov et al.,^[44] Jurisch and Behr,^[45] and Pyatkova et al.,^[46] however, stating that this phase has no solubility in the Si-rich side disagrees with Svechnikov et al.^[44] We found that the Cr₅Si₃ phase has a solubility range that extends toward the Si-rich side. These results

suggest that the Cr₃Si and Cr₅Si₃ phases are not so stable on the Si- and Cr-rich side from the stoichiometric compositions. The thermodynamic assessment is a scope of future studies. The existence of the homogeneity range of the CrSi₂ phase has been suggested by Dudkin and Kuznetsova,^[49] Dubrovskaya and Gel'd,^[48] and Voronov et al.^[47] using the electrical conductivity measurements. However, in this study, we found that the CrSi₂ phase has almost no homogeneity range.

4.5 α - β Transformation of Cr₅Si₃ Phase

Chang^[43] have claimed that there is a phase transformation in the Cr₅Si₃ phase at 1505 ± 20 °C through the DTA measurements, and later, high-temperature β -Cr₅Si₃ and low-temperature α -Cr₅Si₃ phases were adopted in the phase diagram of the Cr-Si system. However, the details of the phase transformation have not been investigated, and the crystal structure of the β -Cr₅Si₃ remains unknown. Figs. 13(a) and (b) show the XRD patterns of Cr-33Si alloy heat-treated at 1600 °C and 1300 °C for 4 h and 7 days, respectively. These peaks are consistent with a mixture of Cr₃Si and α -Cr₅Si₃, as shown in the lower part of Fig. 13. Moreover, no signal was detected by DTA and DSC measurements in Cr-35Si, as shown in Fig. 7(e). Therefore, we concluded that the α - β transformation of the Cr₅Si₃ phase does not occur and that only the α -Cr₅Si₃ exists as the Cr₅Si₃ intermetallic compound.

5 Summary

In this study, the melting temperature of pure Cr and phase equilibria in the Cr-Si binary system were experimentally determined by thermal and equilibrium composition analyses. From the heating curves of the DTA measurements calibrated using pure metals, the melting point of pure Cr was determined to be 1861 ± 3 °C with the consideration of N and O impurities. This melting point is 46 °C lower than the one proposed by the SGTE unary database; however, it correlates, within the range of experimental error, with the latest experiments by Josell et al. and several previous studies. In the Cr-Si binary system, the thermal analysis revealed that the peritectic reaction temperature of liquid \leftrightarrow Cr₅Si₃ + CrSi and liquidus temperature in this concentration range are higher than the reported values. The congruent melting temperature of the CrSi₂ phase was found to be higher. For the Cr₅Si₃ phase, the invariant reaction involving melting was confirmed to be a eutectic reaction of liquid \leftrightarrow Cr₃Si + Cr₅Si₃, and the phase transformation, from the α -Cr₅Si₃ to β -Cr₅Si₃, that has been reported in previous phase diagrams was absent. Equilibrium compositions of two-phase alloys in the whole

concentration range of the Cr-Si system were determined using FE-EPMA/WDS at temperatures between 1200 and 1600 °C. The solubility of Si in the Cr solid solution was determined. We found that the solubility range of the Cr₃Si phase inclines toward the Cr-rich side, whereas the Cr₅Si₃ phase extended toward the Si-rich side. The CrSi₂ phase was a line compound.

Acknowledgments This study was supported by JSPS KAKENHI Grant Number 20H00298 and by JST SPRING, Grant Number JPMJSP2114. The authors thank Mr. Fuyuki Sakamoto (Analytical Research Core for Advanced Materials, Institute of Materials Research, Tohoku University) for ICP-OES analysis.

References

- J.H. Perepezko, The Hotter the Engine, the Better, *Science*, 2009, **326**, p 1068-1069.
- O.N. Senkov, G.B. Wilks, D.B. Miracle, C.P. Chuang, and P.K. Liaw, Refractory High-Entropy Alloys, *Intermetallics*, 2010, **18**, p 1758-1765.
- W. Xia, X. Zhao, L. Yue, and Z. Zhang, A Review of Composition Evolution in Ni-Based Single Crystal Superalloys, *J. Mater. Sci. Technol.*, 2020, **44**, p 76-95.
- H. Long, S. Mao, Y. Liu, Z. Zhang, and X. Han, Microstructural and Compositional Design of Ni-Based Single Crystalline Superalloys - A Review, *J. Alloy. Compd.*, 2018, **743**, p 203-220.
- R.C. Reed, *The Superalloys: Fundamentals and Applications*, Cambridge University Press. U. K, Cambridge, 2008.
- H. Harada, M. Yamazaki, and Y. Koizumi, A Series of Nickel-Base Superalloys on γ - γ' tie Line of Alloy Inconel 713C, *Tetsu-to-Hagane*, 1979, **65**, p 1049-1058.
- K. Li, J. Liu, Y. Wang, and F. Gao, A New Strategy to Toughen NbCr₂ Laves Phase, *Mater. Sci. Technol.*, 2021, **37**(4), p 439-445.
- A.V. Kazantzis, M. Aindow, I.P. Jones, G.K. Triantafyllidis, and J.Th.M. De Hosson, The Mechanical Properties and the Deformation Microstructures of the C15 Laves Phase Cr₂Nb at High Temperatures, *Acta Mater.*, 2007, **55**, p 1873-1884.
- T. Takasugi, M. Yoshida, and S. Hanada, Deformability Improvement in C15 NbCr₂ Intermetallics by Addition of Ternary Elements, *Acta Mater.*, 1996, **44**(2), p 669-674.
- M. Takeyama, and C.T. Liu, Microstructure and Mechanical Properties of Laves-Phase Alloys Based on Cr₂Nb, *Mater. Sci. Eng., A*, 1991, **132**, p 61-66.
- A. Bhowmik, S. Neumeier, J.S. Barnard, C.H. Zenk, M. Göken, C.M.F. Rae, and H.J. Stone, Microstructure and Mechanical Properties of Cr-Ta-Si Laves Phase-Based Alloys at Elevated Temperatures, *Phil. Mag.*, 2014, **94**(34), p 3914-3944.
- A. Bhowmik, and H.J. Stone, Microstructure and Mechanical Properties of Two-Phase Cr-Cr₂Ta Alloys, *Metall. and Mater. Trans. A.*, 2012, **43A**, p 3283-3292.
- A. Soleimani-Dorcheh, and M.C. Galetz, Oxidation-Nitridation Mechanism in Eutectic Cr-Silicide Alloy and Its Mitigation by Germanium Alloying, *Oxid Met.*, 2017, **88**, p 549-564.
- A. Soleimani-Dorcheh, and M.C. Galetz, Oxidation and Nitridation Behavior of Cr-Si Alloys in Air at 1473 K, *Oxid Met.*, 2015, **84**, p 73-90.
- Y. Aono, T. Omori, and R. Kainuma, Microstructure and High-Temperature Strength in Cr-Si Binary Alloys, *Intermetallics*, 2019, **112**, 106526.
- H. Nakasawa, T. Takamatsu, Y. Iijima, K. Hayashi, and Y. Miyazaki, Thermoelectric Properties of Mo and Ge co-Substituted CrSi₂, *Trans. Mater. Res. Soc. Jpn*, 2018, **43**(2), p 85-91.
- T. Dasgupta, J. Etourneau, B. Chevalier, S.F. Matar, and A.M. Umarji, Structural, Thermal, and Electrical Properties of CrSi₂, *J. Appl. Phys.*, 2008, **103**, 113516.
- I. Nishida, The Crystal Growth and Thermoelectric Properties of Chromium Disilicide, *J. Mater. Sci.*, 1972, **7**, p 1119-1124.
- A.T. Dinsdale, SGTE Data for Pure Elements, *Calphad*, 1991, **15**(4), p 317-425.
- J.-O. Andersson, Thermodynamic Properties of Chromium, *Int. J. Thermophys.*, 1985, **6**(4), p 411-419.
- L. Gurvich, I. Veits, V. Medvedev, Calculations of Thermodynamic Properties, T4 (1982) 9-20.
- R. Hultgren, P.D. Desai, D. Hawkins, M. Gleiser, K. Kelley, "Selected Values of the Thermodynamic Properties of the Elements," American Society for Metals, Metals Park, OH (1973).
- H. Okamoto, M. Schlesinger, E. Mueller, "ASM Handbook Volume 3: Alloy Phase Diagrams," ASM International, Materials Park, OH (1992).
- G. Grube, and R. Knabe, *Zeitschrift für Elektrochemie*, 1936, **42**, p 793-804.
- S.J. Carlisle, J.W. Christian, and W. Hume-Rothery, The Equilibrium Diagram of the System Chromium-Manganese, *J. Inst. Met.*, 1949, **76**(2), p 169-194.
- J.W. Putman, R.D. Potter, and N.J. Grant, The Ternary System Chromium-Molybdenum-Iron, *Transactions of American Society for Metals*, 1951, **43**(2), p 824-852.
- D.S. Bloom, and N.J. Grant, Chromium-Nickel Phase Diagram, *J. Metals*, 1951, **3**(2), p 1009-1014.
- H.T. Greenaway, S.T.M. Johnstone, and M.K. McQuillan, High Temperature Thermal Analysis Using the Tungsten-Molybdenum Thermocouple, *J. Inst. Met.*, 1951, **80**, p 109-114.
- D.S. Bloom, and N.J. Grant, Chromium-Nickel Phase Diagram, *Trans. AIME*, 1952, **194**, p 523-524.
- D.S. Bloom, J.W. Putman, and N.J. Grant, Melting Point and Transformation of Pure Chromium, *J. Metals*, 1952, **4**, p 626.
- C.W. Haworth, and W. Hume-Rothery, The Constitution of Molybdenum-Rhodium and Molybdenum-Palladium Alloys. Appendix: the Construction of Two Laboratory Furnaces for Use Above 2000°C, *Journal Inst. Metals*, 1959, **87**, p 265-272.
- V.M. Pan, Collection of Scientific Works of the Institute of Metal Physics of the Academy of Sciences of the Ukrainian SSR, 1964, N 20, p. 130.
- N.A. Nedumov, and V.K. Grigorovich, *In the book: High-temperature inorganic compounds: Collection of the Institute of Problems of Metallurgy of the Academy of Sciences of the USSR Naukova Dumka, Kiev*, 1965, p 25
- E. Rudy, St. Windisch, "The Phase Diagrams Hafnium-Vanadium and Hafnium-Chromium," *Journal of the Less-Common Metals* 15 (1) (1968) 13-27.
- M. Pirani, and H. Alterthum, A Method for Determining the Melting Point on High-Melting Metals, *Zeitschrift für Elektrochemie*, 1923, **29**, p 5-8.
- E. Rudy, and J. Progulski, A Pirani Furnace for the Precision Determination of the Melting Temperatures of Refractory Metallic Substances, *Planseeberichte für Pulvermetallurgie*, 1967, **15**(1), p 13-45.
- D. Josell, D. Basak, J.L. McClure, U.R. Kattner, M.E. Williams, W.J. Boettinger, and M. Rappaz, (2001) Moving the pulsed heating technique beyond monolithic specimens: Experiments with coated wires", *J. Mater. Res.*, 2001, **16**(8), p 2421-2428.
- S. Cui, and I.-H. Jung, Thermodynamic Assessments of the Cr-Si and Al-Cr-Si Systems, *J. Alloy. Compd.*, 2017, **708**, p 887-902.

39. H. Chen, Y. Du, and J.C. Schuster, On the Melting of Cr_5Si_3 and Update of the Thermodynamic Description of Cr-Si, *Calphad*, 2009, **33**(1), p 211-214.
40. Y. Du, and J.C. Schuster, Experimental Reinvestigation of the CrSi-Si Partial System and Update of the Thermodynamic Description of the Entire Cr-Si System, *J. Phase Equilibria*, 2000, **21**(3), p 281-286.
41. C.A. Coughanowr, and I. Ansara, Assessment of the Cr-Si System, *Calphad*, 1994, **18**(2), p 125-140.
42. P. Pfizenmaier, A.S. Ulrich, M.C. Galetz, and U. Glatzel, Determination of Heat Treatment Parameters by Experiments and CALPHAD for Precipitate Hardening of Cr-Alloys with Si, Ge and Mo, *Intermetallics*, 2020, **116**, 106636.
43. Y.A. Chang, Phase Relationships in the System Chromium-Silicon, *Trans. Metall. Soc. AIME*, 1968, **242**, p 1509-1515.
44. V.N. Svechnikov, Y.A. Kocherzhinskii, and L.M. Yupko, Chromium-Silicon Phase Diagram, *Sb. Nauchn. Rab Inst. Metallofiz. Akad. Nauk. Ukr. SSR*, 1964, **19**, p 212-218.
45. M. Jurisch, and G. Behr, Growth and Perfection of Chromium-Silicon (Cr_3Si) Single Crystals, *Acta Phys. Acad. Sci. Hung.*, 1979, **47**, p 201-207.
46. T.M. Pyatkova, V.I. Surikov, A.K. Shtolyts, V.L. Zagryazhskii, and P.V. Gel'd, β -Phase Homogeneity Region of a Chromium-Silicon System and Mutual Solubility of Cr_3Si and V_3Si , *Izv. Akad. Nauk SSSR Neorg. Mater.*, 1971, **7**(10), p 1755-1758.
47. B.K. Voronov, L.D. Dudkin, N.I. Kiryukhina, and N.N. Trusova, Investigation of the Cr-Si System in the Disilicide Region, *Sov. Powder Metall. Met. Ceram.*, 1967, **49**(1), p 56-61.
48. L.B. Dubrovskaya, and P.V. Gel'd, Boundaries of the Homogeneity Region and Nature of Chromium Disilicide, *Russ. J. Inorg. Chem.*, 1963, **8**(7), p 854-857.
49. L.D. Dudkin, and E.S. Kuznetsova, Investigation of the Electro-physical Properties of Alloys Based on Semiconductor Disilicides of Chromium and Manganese, *Sov. Powder Metall. Met. Ceram.*, 1962, **12**(6), p 20-31.
50. R.G. Ross, and W. Hume-Rothery, High Temperature x-ray Metallography. I. A New Debye-scherrer Camera for Use at Very High Temperatures II. A New Para-focusing Camera III. Applications to the Study of Chromium, Hafnium, Molybdenum, Rhodium, Ruthenium and Tungsten, *Journal of The Less-Common Metals*, 1963, **5**(3), p 258-270.
51. R. Kieffer, F. Benesovsky, and H. Schroth, The System Chromium-Silicon and Solid Solutions of Silicides, *Z. Met.*, 1953, **44**, p 437-442.
52. C.H. Dauben, D.H. Templeton, and C.E. Myers, The Crystal Structure of Cr_5Si_3 , *J. Phys. Chem.*, 1956, **60**, p 443-445.
53. B. Boren, X-ray study on alloys of silicon with chromium, manganese, cobalt and nickel, "Arkiv. Kemi, Mineral. Geol. 11A 28 (1933)
54. W.M. Yim, and R.J. Paff, Thermal Expansion of AlN, Sapphire, and Silicon, *J. Appl. Phys.*, 1974, **45**(3), p 1456-1457.
55. W. Xiong, M. Selleby, Q. Chen, J. Odqvist, and Y. Du, Phase Equilibria and Thermodynamic Properties in the Fe-Cr System, *Crit. Rev. Solid State Mater. Sci.*, 2010, **35**(2), p 125-152.
56. A. Obaied, B. Bocklund, S. Zomorodpoosh, L. Zhang, R. Otis, I. Zi-Kui Liu, and Roslyakova, Thermodynamic Re-Assessment of Pure Chromium Using Modified Segmented Regression Model, *Calphad*, 2020, **69**, p 1017.

Publisher's Note Springer Nature remains neutral with regard to jurisdictional claims in published maps and institutional affiliations.